Supporting Information

Autoluminescent Metal-Organic Frameworks: self-photoemission of a highly stable thorium MOF.

Jacopo Andreo[†*], Emanuele Priola[†], Gabriele Alberto[†], Paola Benzi[†‡], Domenica Marabello[†‡], Davide M. Proserpio[¤¢], Carlo Lamberti[‡#§] and Eliano Diana[†‡*]

[†] Department of Chemistry, University of Turin, Via Pietro Giuria 7, 10125, Turin, Italy.
[‡] CriSDi, Interdepartmental Center for Crystallography, Via Pietro Giuria 7, 10125, Turin, Italy.
[¤]Dipartimento di Chimica, Università degli Studi di Milano, Via Golgi 19, 20133 Milano, Italy.
[¢]Samara Center for Theoretical Materials Science (SCTMS), Samara State Technical University, Molodogvardeyskaya St. 244, Samara 443100, Russia.
[#] Department of Physics, Interdepartmental NIS Centre, University of Turin, Via Pietro Giuria 1, 10125, Turin, Italy.
[§] IRC "Smart Materials", Southern Federal University, Zorge Street 5, Rostov-on-Don, Russia.

X-ray Structure determination and structural data

X-ray diffraction data for compound $Th(NDC)_2$ were collected at room temperature using an Oxford Diffraction Gemini R Ultra diffractometer with mirror monochromatized Cu-Kα radiation (1.5418 Å). The CrysAlisPro[1] package was used for data collection and integration, SHELXT [2] for resolution, SHELXL[2] and Olex2[3] for refinement, Vesta 3[4] for graphics. All but the hydrogen atoms were anisotropically refined. All H atoms were calculated and refined riding with U_{iso}=1.2 U_{eq} of the bonded atom. ToposPro 5.1[5] has been used for topological analysis and for graphical representation of the Underlying Net, while Mercury 3.9[6] and CrystalExplorer[7] for the empty space analysis of the structure. The void space has been studied with two approaches: with Mercury 3.9, the contact surface in the Corey-Pauling-Koltun representation of the crystal, using a probe radius of 1.2 A° and a space grid of 0.1 A°, has been calculated[8], and with CrystalExplorer with a method based on the isosurface of the procrystal electron density (mapped at a value of 0.002 e)[9]. The structure was deposited on CSD databank with CCDC 1548792. Details on crystal data and refinement details are reported in Table 1s.

Empirical formula	$C_{24}H_{12}O_8Th$
Formula weight	660.38
Temperature/K	293(2)
Crystal system	monoclinic
Space group	C2/c
a/Å	17.7914(5)
b/Å	22.1948(6)
c/Å	12.5214(3)
α/°	90
β/°	108.913(3)
γ/°	90
Volume/$Å^3$	4677.5(2)
Z	8
ρ_{calc}g/cm^3	1.876
μ/mm^{-1}	20.968
F(000)	2480.0
Crystal size/mm^3	0.1 × 0.04 × 0.01
Radiation	CuKα (λ = 1.54184)
2Θ range for data collection/°	6.59 to 115.804

Index ranges	$-19 \leq h \leq 19, -24 \leq k \leq 24, -13 \leq l \leq 13$
Reflections collected	14439
Independent reflections	3230 [$R_{int} = 0.0305$, $R_{sigma} = 0.0232$]
Data/restraints/parameters	3230/0/298
Goodness-of-fit on F^2	1.053
Final R indexes [I>=2σ (I)]	$R_1 = 0.0206$, $wR_2 = 0.0450$
Final R indexes [all data]	$R_1 = 0.0360$, $wR_2 = 0.0513$
Largest diff. peak/hole / e $Å^{-3}$	1.08/-0.53

Table S1: Crystal Data and Refinement details for $Th(NDC)_2$.

Atom1	Atom2	Atom3	Angle (°)		Atom1	Atom2	Length (A°)
O1A	Th1	O1B	101.0(1)		Th1	O1A	2.310(3)
O1A	Th1	O1C	143.5(1)		Th1	O1B	2.332(4)
O1A	Th1	O2A	73.7(1)		Th1	O1C	2.401(4)
O1A	Th1	O3A	143.5(1)		O1A	C1A	1.256(6)
O1A	Th1	O4A	78.3(1)		O2A	C1A	1.259(6)
O1A	Th1	O2B	73.0(1)		O3A	C12A	1.263(7)
O1A	Th1	O2C	77.0(1)		O4A	C12A	1.255(7)
O1B	Th1	O1C	86.3(1)		O1B	C1B	1.274(7)
O1B	Th1	O2A	73.5(1)		O2B	C1B	1.243(6)
O1B	Th1	O3A	77.0(1)		O1C	C1C	1.273(7)
O1B	Th1	O4A	143.2(1)		O2C	C1C	1.252(6)
O1B	Th1	O2B	73.0(1)		C1A	C2A	1.496(9)
O1B	Th1	O2C	141.1(1)		C2A	C3A	1.407(8)
O1C	Th1	O2A	74.3(1)		C2A	C11A	1.364(8)
O1C	Th1	O3A	73.1(1)		C3A	C4A	1.36(1)
O1C	Th1	O4A	74.9(1)		C4A	C5A	1.405(8)
O1C	Th1	O2B	142.1(1)		C5A	C6A	1.41(1)
O1C	Th1	O2C	118.6(1)		C5A	C10A	1.411(9)
O2A	Th1	O3A	136.9(1)		C6A	C7A	1.375(8)
O2A	Th1	O4A	71.0(1)		C7A	C8A	1.420(9)
O2A	Th1	O2B	126.3(1)		C7A	C12A	1.492(9)
O2A	Th1	O2C	138.8(1)		C8A	C9A	1.37(1)
O3A	Th1	O4A	124.9(1)		C9A	C10A	1.420(9)
O3A	Th1	O2B	71.6(1)		C1B	C2B	1.478(9)
O3A	Th1	O2C	82.4(1)		C2B	C3B	1.374(9)
O4A	Th1	O2B	138.3(1)		C2B	C6B	1.41(1)
O4A	Th1	O2C	75.2(1)		C3B	C4B	1.41(1)
O2B	Th1	O2C	69.3(1)		C4B	C5B	1.410(9)
Th1	O1A	C1A	169.9(4)		C1C	C2C	1.492(9)
C1A	O2A	Th1	129.8(4)		C2C	C3C	1.355(7)
C10A	O3A	Th1	142.1(4)		C2C	C5C	1.41(1)
C10A	O4A	Th1	135.5(4)		C3C	C4C	1.406(9)
Th1	O1B	C1B	163.8(4)		C5C	C6C	1.36(1)
C1B	O2B	Th1	134.6(4)		C11A	C10A	1.40(1)

Table S2: Selected Bond and angles for $Th(NDC)_2$.

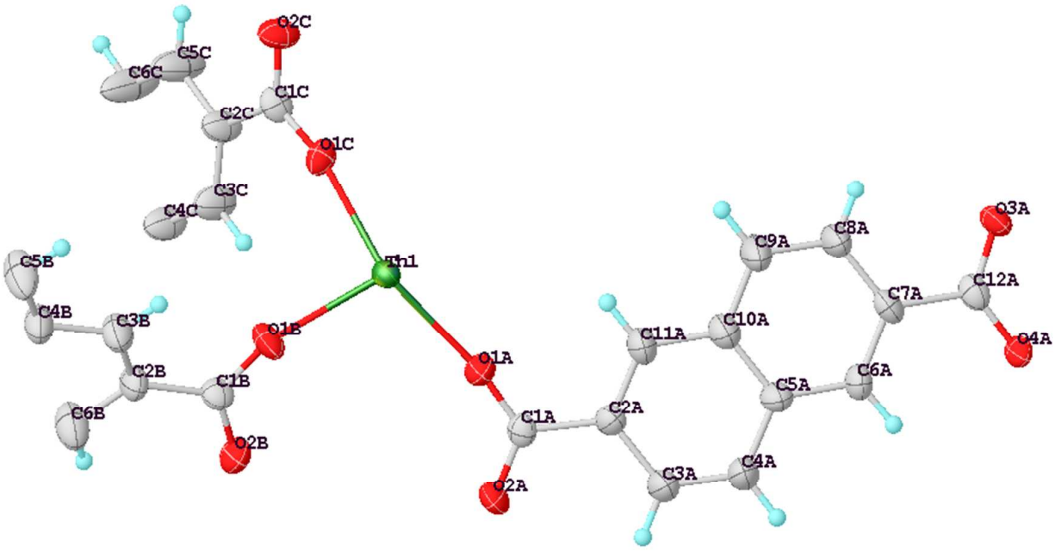

Figure S1: Asymmetric unit of compound $Th(NDC)_2$, with thermal ellipsoids at 50% probability.

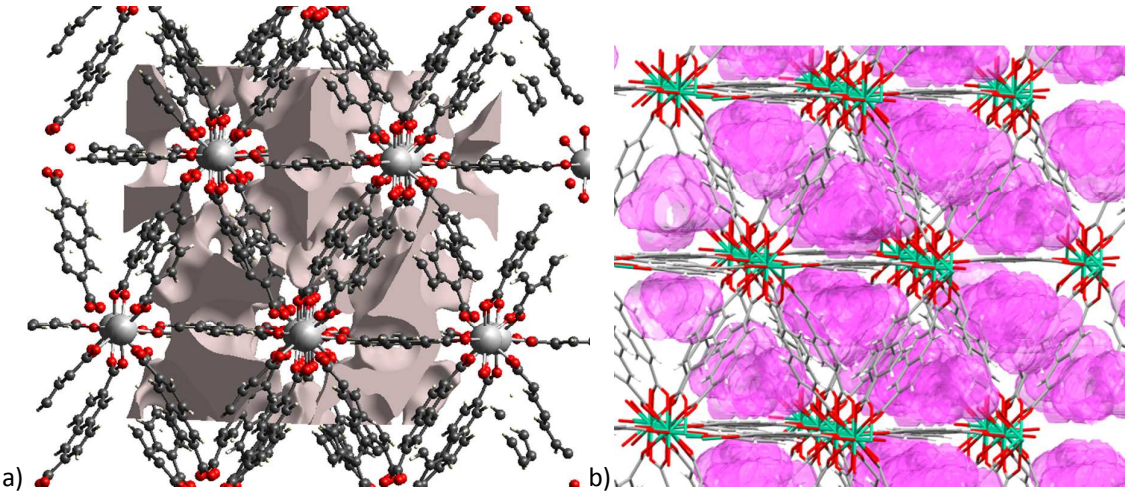

c)

	Empty volume (Å^3)	Percentage of empty volume
Hirshfeld Surface approach	1188,09	25.4%
Contact surface approach in the Corey-Pauling-Koltun representation of the crystal	940.39	20.1%

Figure S2: a) Representation of the empty space calculated by the Hirshfeld surface approach (isovalue 0.002 e) and b) contact surface calculated with a probe radius of 1.2 Å and a grid of 0.1 Å. c) table of the value of empty space calculated from these two approaches.

Topological analysis of the underlying Net

The rod-MOF $Th(NDC)_2$ is described by a new binodal 6-c net with point symbol $(3.4^2.5^7.6^5)(3^2.4^2.5^5.6^4.7^2)$. The parallel rods consist of ThO_8 -$Th(COO)_4$Th- packed into a hexagonal pattern (6-c **hxl**) in the (1,0,1) projection. The rod is built by two independent nodes.

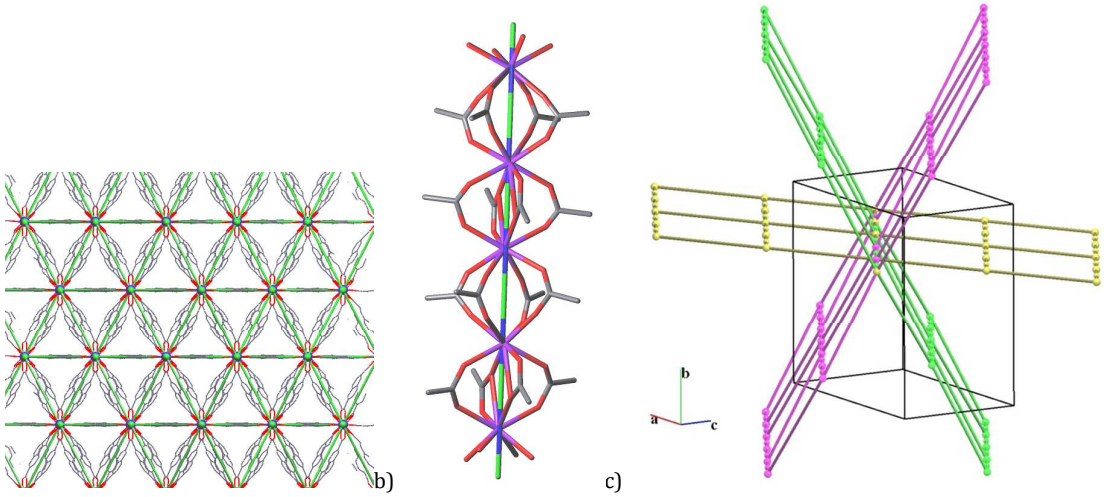

Figure S3: (a) hexagonal pattern (6-c **hxl**) in the (1,0,1) projection, (b) basic rod forming the topology and (c) the three non-equivalent planes around each rod.

The rods are reciprocally shifted, and the links are not orthogonal to the rods (in such case it would be pcu net). In the view along the rods (1,0,1) there are 3 planes: the unique (0,0,1), and the other two equivalent by symmetry (1,1,-1)(1,-1,-1). In the plane (0,0,1) the ligands are almost planar and lay in one plane connecting only half the nodes of rods, here the rods are shifted by 4.40 Å that is almost the distance between metal atoms in the rod, 4.53 Å. The links allocated in the parallel lines form an angle with rods in 69°. The distance between the rods in the plane is 11.62 Å.

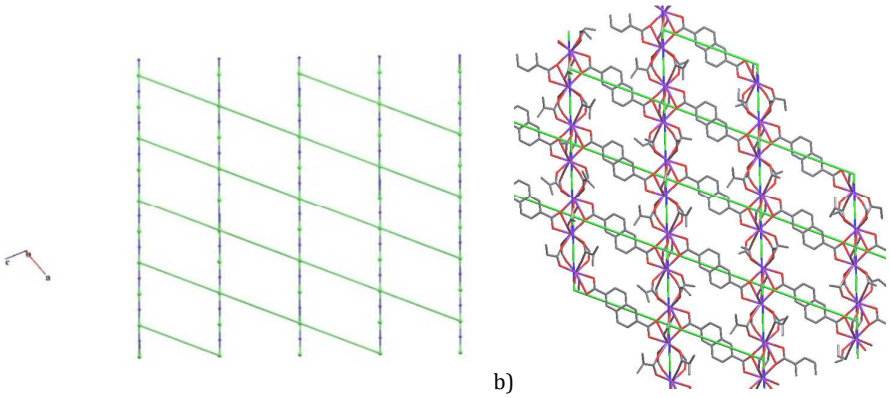

Figure S4: Representation of the topology of single plane (0,0,1) (a) and its superposition on crystal structure (b).

In the two equivalent planes (1,1,-1)(1,-1,-1) the ligands are distorted (non-planar) and located out of plane, but the underlying net is planar. Links connect 3/4 nodes of rods. Here the rods are shifted on 2.20 Å that is almost the half of the distance between metal atoms in the rod. The links are allocated in the two sets of parallel lines and they form two angles with rods in 80.0 ° and 100.5 °. The distance between the rods in the planes is larger, 12.53 Å, than in (0 0 1) plane.

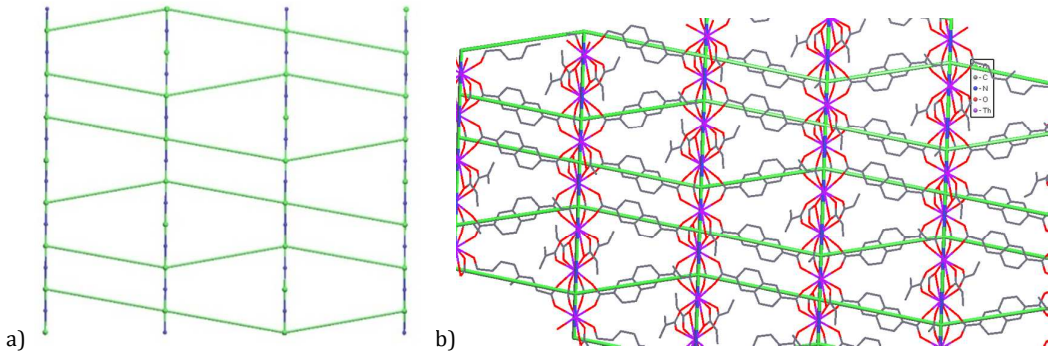

Figure S5: Representation of the topology of the two symmetry equivalent planes (1,1,-1)(1,-1,-1) (a) and its superposition on crystal structure (b).

The terephthalate $Th(BDC)_2$ BDC=benzene dicarboxylate derivative is described by a more symmetric rod-MOF , the uninodal 6-c net **rob** with point symbol $(4^8.6^6.8)$. (http://rcsr.net/nets/rob) Here also the parallel rods consist of ThO_8 - $Th(COO)_4Th$- packed into an hexagonal lattice (6-c **hxl**), but now the rod is formed by a single node. [POXLEV[10]; POXLEV01[11]]

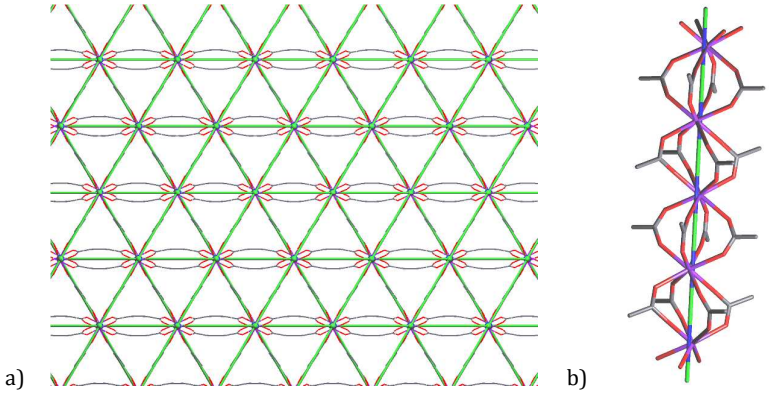

Figure S6: Representation of the underlying net of $Th(BDC)_2$ (a) and fundamental structure of its rod (b).

The 3 planes are now more symmetric, the single one is rectangular but with the ligands out of plane

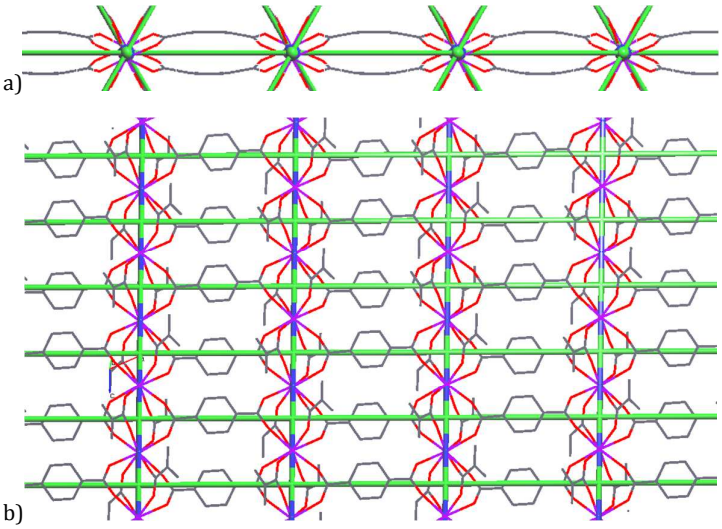

Figure S7: Representations of the underlying net of the plane (0,1,0) in $Th(BDC)_2$.

The other two equivalent planes are with the ligands perfectly sitting in the planes, and resemble the unique (1,0,0) plane of the naphthalene derivative (see figure above).

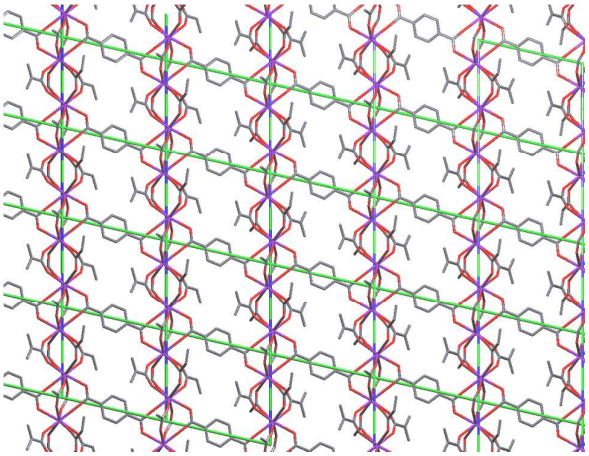

Figure S8: Representation of the underlying net of the two equivalent perpendicular planes in $Th(BDC)_2$ resembling the unique (1,0,0) plane of the naphthalene derivative.

The coordinates of the idealized new net are:

CRYSTAL

NAME "Th(BDC)2 new binodal 6-c"

GROUP I12/a1

CELL 1.79606 1.44800 2.00001 90.0000 94.8953 90.0000

NODE 1 6 0.25000 0.75000 0.25000

NODE 2 6 0.25000 0.34808 0.00000

EDGE 0.25000 0.34808 0.00000 0.75000 0.25000 0.25000

EDGE 0.25000 0.75000 0.25000 0.25000 0.75000 -0.25000

EDGE 0.25000 0.34808 0.00000 0.25000 -0.25000 0.25000

EDGE 0.25000 0.34808 0.00000 0.75000 0.65192 0.00000

EDGE_CENTER 0.50000 0.29904 0.12500

EDGE_CENTER 0.25000 0.75000 0.00000

EDGE_CENTER 0.25000 0.04904 0.12500

EDGE_CENTER 0.50000 0.50000 0.00000

END

X-ray powder diffraction

Powder diffractograms were recorded with Oxford Diffraction Gemini R Ultra diffractometer using Cu-Kα radiation in a transmitting mode on a spherical small powder sample mounted on a glass capillary.

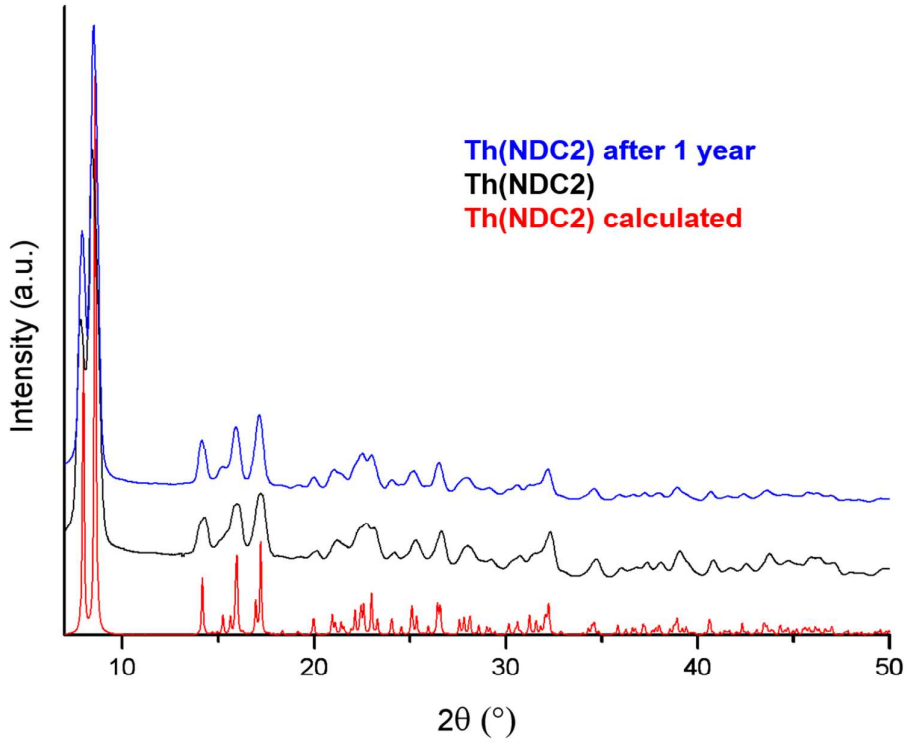

Figure S9: Comparison between the powder diffraction of $Th(NDC)_2$, the calculated diffractogram and the MOF aged 1 year.

Vibrational data

FT-Raman spectra were recorded for all products with a Bruker Vertex 70 spectrometer, equipped with the RAMII accessory. Raman spectra were recorded from crystalline or powder samples by exciting with a 1064 nm laser, with a resolution of 4cm-

Frequence region (cm^{-1})	2,6-naphthalenedicarboxylic Acid		Th(NDC)2	
	Raman (cm^{-1})	IR (cm^{-1})	Raman (cm^{-1})	IR (cm^{-1})
3500 -2500	3086, 3063	3056, 2960, 2876, 2827, 2640, 2554	3054, 3048	3369
2500 -1500	1636, 1577	1669, 1602, 1574, 1507	1638, 1595	1657, 1609, 1568
1500 -1000	1481, 1440, 1407, 1390, 1342, 1293, 1230, 1157, 1111	1423, 1374, 1340, 1288, 1265, 1187, 1141, 1095	1481, 1394, 1242, 1151, 1125	1492, 1403, 1362, 1205, 1144, 1104
1000 -500	968, 909, 838, 822, 769, 643, 525	916, 827, 775, 749, 642, 556	973, 781, 521	922, 793, 773, 587, 531
500 -50	398, 332, 239, 191, 107, 107, 76	472, 426, 380, 299, 244, 185, 77	407, 72	452, 395, 348, 298, 200, 159

[1]. ATR spectra were obtained with a Bruker Vertex 70 spectrophotometer equipped with Harrick MVP2 ATR cell.

Table S3: List of observed vibrational (IR and Raman) bands.

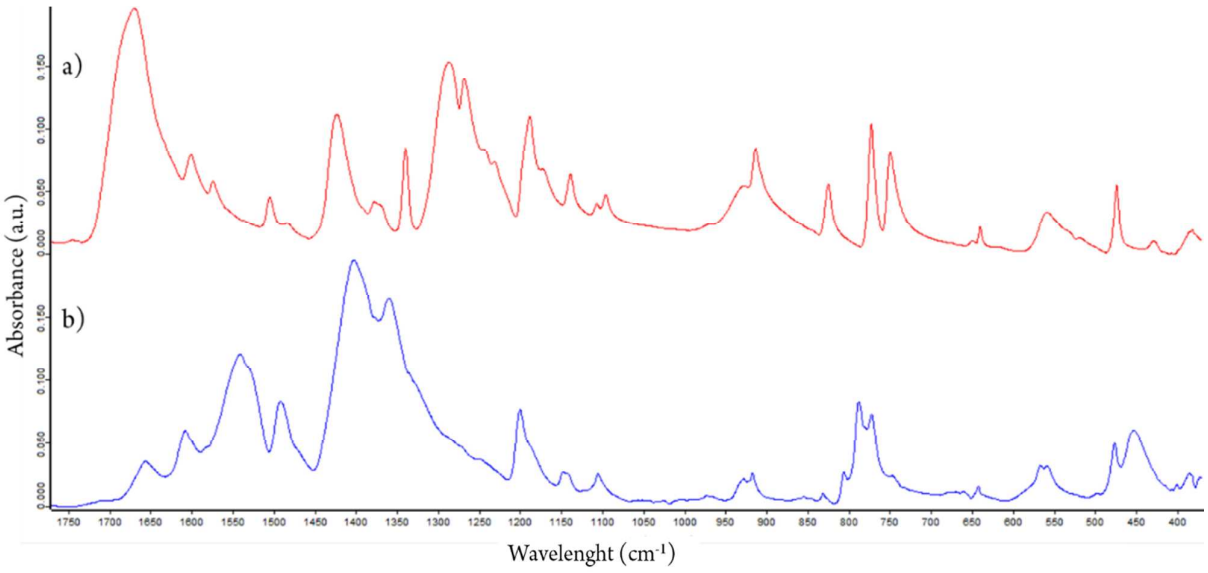

Figure S10: IR spectra of $Th(NDC)_2$ (blue) and 2,6-naphthanendicarboxylic acid (red).

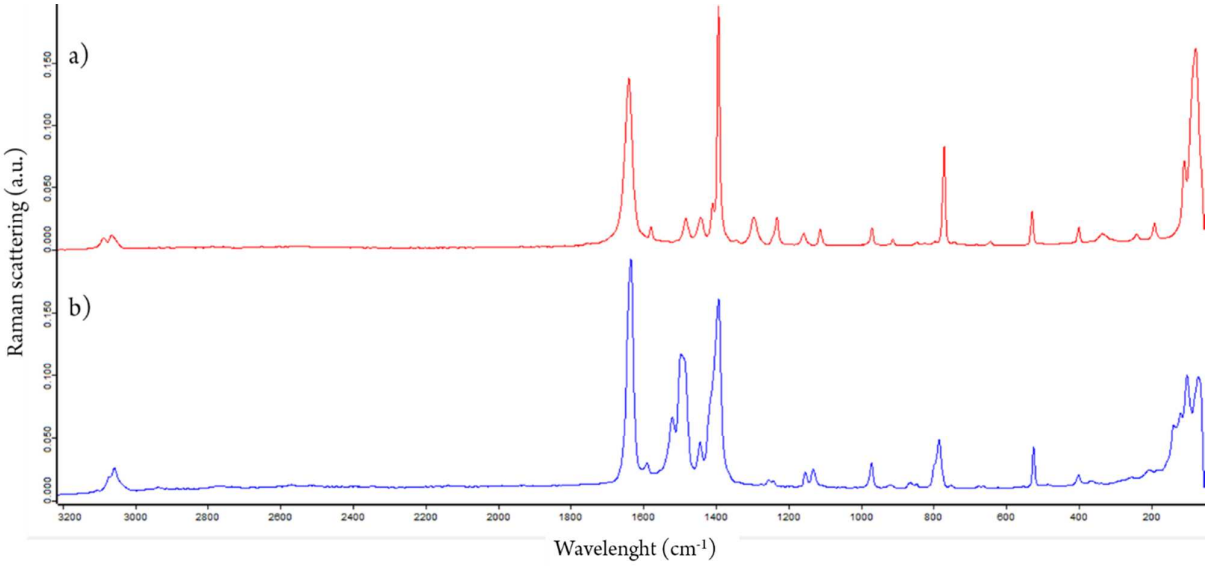

Figure S11: Raman spectra of $Th(NDC)_2$ (blue) and 2,6-naphthanendicarboxylic acid (red).

TGA Analysis

Thermal stability was evaluated with a Hi-Res thermogravimetric analyzer (TGA Q500 balance, TA Inc.) on 10 mg sample contained in alumina pans, with a 10°C/min heating ramp from 50 to 800°C under a 100 cm^3/min air flow.

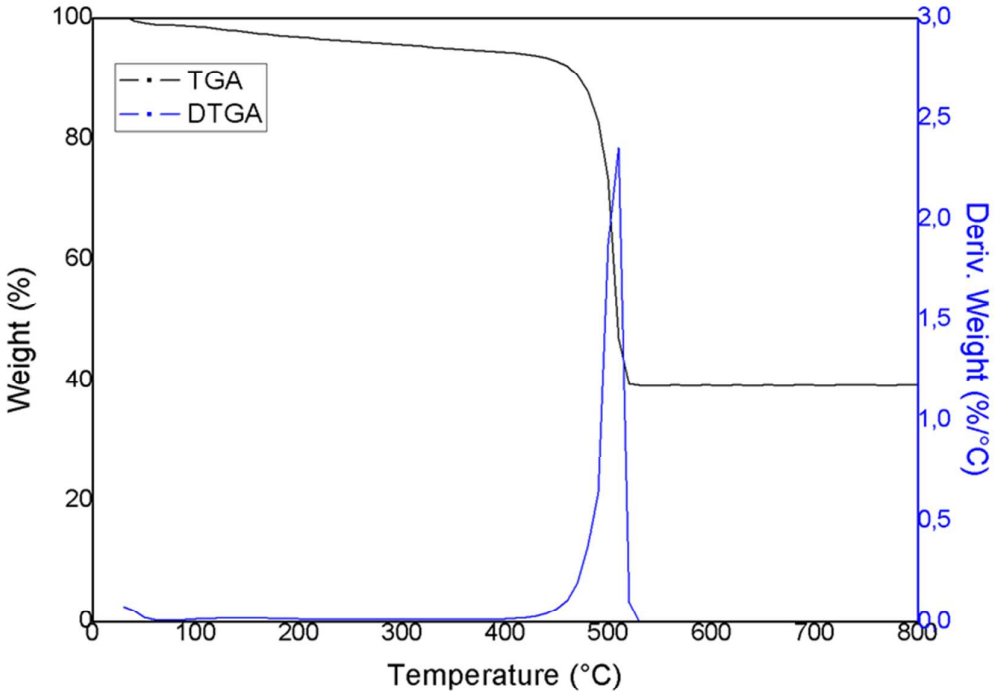

Figure S12: Thermogram of Th(NDC)2 (black line) and derivative (blue line)

UV-Vis Spectroscopy

Electronic absorption spectra were collected with a Varian Cary 5000 spectrophotometer. In the case of dried NPs samples, an integrating sphere coated with Spectralon (also used as reference) was inserted for measurements in the diffuse reflectance mode. The reflectance spectra were then converted to absorbance-like profiles by using the Kubelka-Munk function.

Photoemission/excitation steady-state spectra were acquired with a Horiba Jobin Yvon Fluorolog 3 TCSPC spectrofluorimeter equipped with a 450-W Xenon lamp and a Hamamatsu R928 photomultiplier.

Fluorescence lifetimes were measured using a time-correlated single photon counting (TCSPC) technique (Horiba Jobin Yvon) with excitation source NanoLed at 297 nm (Horiba) or at 370 nm (Horiba) and impulse repetition rate of 1 MHz at 90 degrees to a TBX-4 detector. The detector was set to the maximum of emission for the compound in exam, with a 5 nm band-pass. The instrument was set in the Reverse TAC mode, where the first detected photon represented the start signal by the time-to-amplitude converter (TAC), and the excitation pulse triggered the stop signal. DAS6 decay analysis software was used for lifetime calculation.

BET analysis

Porosity was evaluated using a Micromeritics ASAP 2020 porosimeter (Micromeritics, Italy), by adsorption of an inert gas (krypton (Kr), for low SSA) at 77 K. Before measurements, all samples were activated in vacuo (residual pressure, 1023 torr) at room temperature for 12 h in order to remove all possible adsorbed atmospheric contaminants.

Computational details

The NDC and thorium NDC salt have been computed with a DFT approach, by using the hybrid B3LYP functional. We used the 6-311+g(d,p) basis set for C,H and O, and the LANL2DZ basis set and pseudopotential for The molecular geometries have been optimized and the minimum of energy checked by examining the harmonic vibrational frequencies. The excited states have been computed by employing the time-dependent DFT approach, with the same basis set and B3LYP functional. All the computation has been performed with the Gaussian 09 package[12].

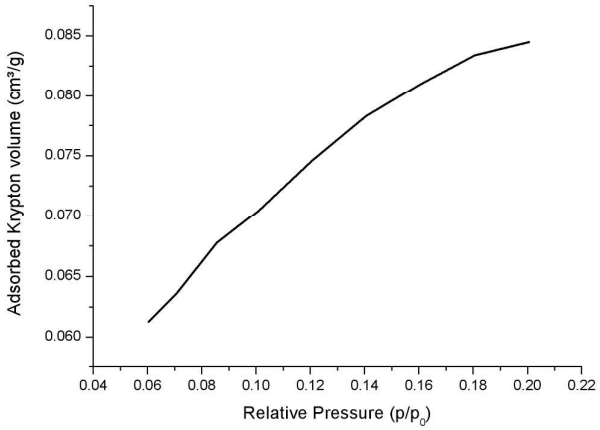

Figure S13: Krypton isotherm at 77 K.

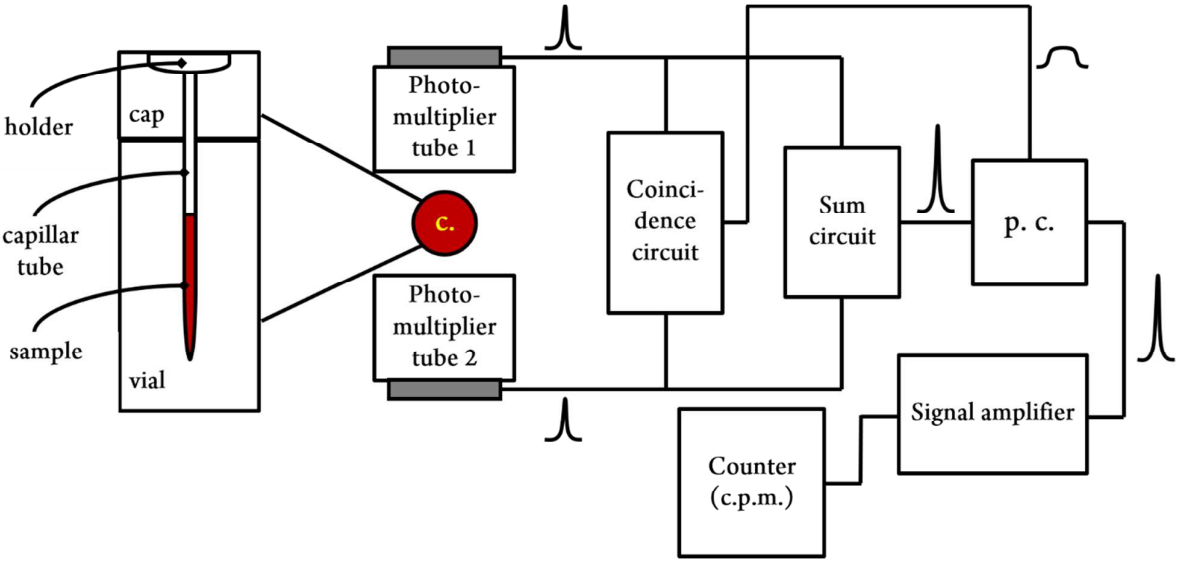

Autoluminescence evaluation

Figure S14: schematic representation of the sample geometry utilized in the autoluminescence measurements and the circuit scheme of the Packard scintillometer.

Autoluminescence measurements counts and errors

All the calculations below exemplify our data treatment. Table S3 reports all the numerical data, although the numerical treatment is not reported it is the same for every experiment[13].

Error determination for $Th(NDC)_2$ autoluminescence:

Counts $Th(NDC)_2$ = 1969543

Minutes of measurement = 958

Counts $Th(NDC)_2$ corrected for the background = Counts $Th(NDC)_2$ – (31*minutes of measurement) = 1939845

$2\sigma\ Th(NDC)_2 = 2\sqrt[2]{\text{Counts Th(NDC)2}} = 2785.57$

mg $Th(NDC)_2$ = 11.7 mg

c.p.m. $Th(NDC)_2$= counts / minutes = 2024.89

Error c.p.m. = 2.90

c.p.m. / mg MOF = 173.0

Error C.P.M. / mg MOF = 0.24

% Error = 1.4%

α particle/autoluminescence respond ratio for $Th(NDC)_2$:

Th specific activity: 1.10 10-7 Ci/g or 4070 Bq/g or 4.07

mg of Th per mg of $Th(NDC)_2$: 0.35 mg

Activity of the sample: 4.07 Bq/mg x 0.35 mg = 1.43 Bq or counts/s

Activity of the sample in counts per minute: 1.43 Bq x 60 s/min = 85.8 counts per minute

Experimental counts: 173.0 counts per minute

Ratio experimental/calculated: 2.016 ≈ 200%

Sample	c.p.m.	2σ	Time (minutes)	Mass (mg)	Norm. c.p.m.	2σ	Mass Th/mg	Ratio exp./calc.
NaF (background)*	31.0	0.5	540	-	-	-	-	-
2,6-NDCA	0.3	0.1	150	-	-	-	-	-
$Th(NO_3)_4{\cdot}5H_2O$	231.1	1.3	541	21.2	10.9	0.06	0.42	0.107
$Th(NDC)_2$	2024.9	2.9	958	11.7	173.0	0.24	0.35	2.016
Th/2,6-NDCA mix	1493.1	3.3	540	15.8	94.5	0.21	0.23	1.683
$Th(NDC)_2$ with liquid scintillator	2892.3	4.6	540	11.7	247.2	0.39	0.35	2.88
$Th(NDC)_2$ with dark paper	196.4	1.2	539	11.7	16.8	0.10	0.35	0.20
$Th(NDC)_2$ after 1 year	2025.2	4.7	361	11.7	173.1	0.40	0.35	2.017
$Th(bdc)_2(DMF)_2$	71,6	0.8	480	1.5	47.7	0.5	0.32	0.61
$Th_6O_4(OH)_4(H_2O)_6(bdc)_6 {\cdot}6DMF{\cdot}12H_2O$	104,0	1.8	120	2.5	41.6	0.7	0.42	0.41

Table S4: Autoluminescence data and errors. *As the NaF was used a s a background it is reported its rough value.

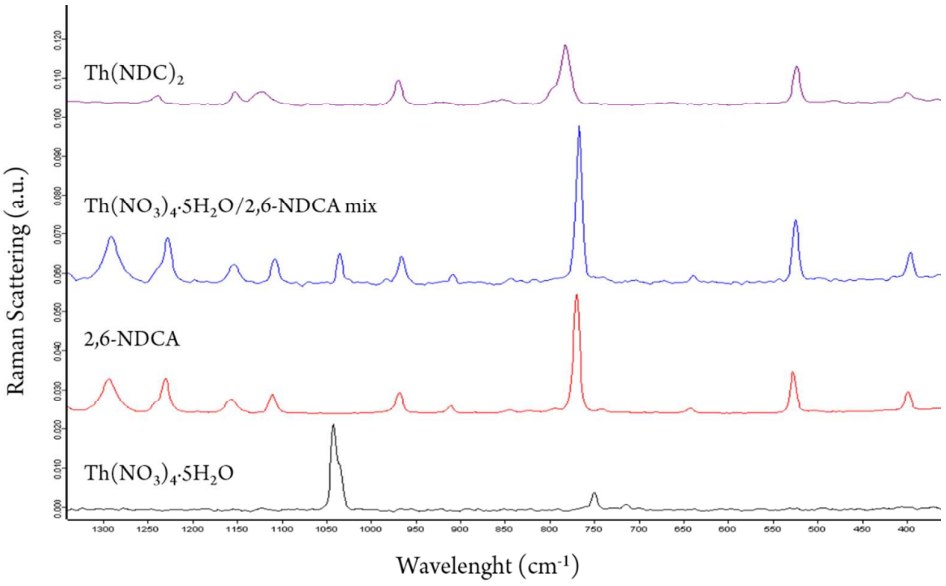

Figure S15: Raman spectra of $Th(NO_3)_4 \cdot 5H_2O$, 2,6-NDCA, Th/2,6-NDCA mix and $Th(NDC)_2$. It is deducible that there is no solid-state reaction between the thorium and the dicarboxylic acid, as the spectrum of the mixture is a sum of the spectra of the components and strongly differs from the spectrum of the mixture.

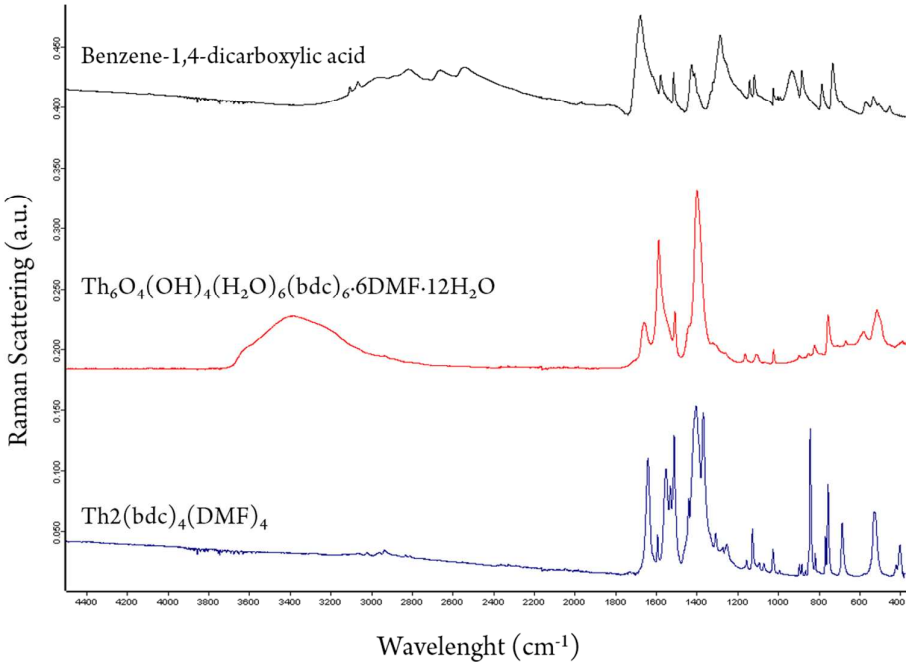

Figure S1: Raman spectra of benzene-1,4-dicarboxylic acid, $Th_6O_4(OH)_4(H_2O)_6(bdc)_6 \cdot 6DMF \cdot 12H_2O$ and $Th2(bdc)_4(DMF)_4$

.

Bibliography

1) CrysAlisPro, Agilent Technologies, Version 1.171.37.31 (release 14-01-2014 CrysAlis171 .NET, compiled Jan 14 2014,18:38:05)
2) Sheldrick G.M. *Acta Cryst. A* **2015**, *71*, 3-8
3) Dolomanov O.V.; Bourhis L. J.; Gildea R. J.; Howard J. A. K.; Puschmann H. *J. Appl. Cryst.* **2009**, *42*, 339-341
4) Momma K.; Izumi F. *J. Appl. Crystallogr.* **2011**, *44*, 1272-1276
5) Blatov V. A.; Shevchenko A. P.; Proserpio D. M. *Cryst. Growth Des.* **2014**, *14*,3576-3
6) Macrae C. F.; Edgington P. R.; McCabe P.; Pidcock E.; Shields G. P.; Taylor R.; Towler M.; Van de Streek J. *J. Appl. Cryst.* **2006**, *39*, 453-457
7) Spackman M.A.; Jayatilaka D. *CrystEngComm* **2009**, *11*, 19-32
8) Connolly M.L. *J.Am.Chem.Soc.* **1985**, *107,* 1118-1124
9) Turner M.J.; McKinnon J.J.; Jayatilaka D.; Spackman M.A. *CrystEngComm* **2011**, *13*, 1804-1813.
10) Falaise C.; Charles J. S.; Volkringer C.; Loiseau T. *Inorg. Chem.* **2015**, *54*, 2235-2242.
11) Zhang Y.; Kadi F.; Karatchevtseva I.; Price J. R.; Li F.; Bhad-Bhade M.; Lu K.; Lumpkin G. R. *J. Incl. Phenom. Macrocycl. Chem.* **2015**, *82*, 163–172.
12) Gaussian 09, Revision D.01,M. J. Frisch, G. W. Trucks, H. B. Schlegel, G. E. Scuseria, M. A. Robb, J. R. Cheeseman, G. Scalmani, V. Barone, B. Mennucci, G. A. Petersson, H. Nakatsuji, M. Caricato, X. Li, H. P. Hratchian, A. F. Izmaylov, J. Bloino, G. Zheng, J. L. Sonnenberg, M. Hada, M. Ehara, K. Toyota, R. Fukuda, J. Hasegawa, M. Ishida, T. Nakajima, Y. Honda, O. Kitao, H. Nakai, T. Vreven, J. A. Montgomery, Jr., J. E. Peralta, F. Ogliaro, M. Bearpark, J. J. Heyd, E. Brothers, K. N. Kudin, V. N. Staroverov, T. Keith, R. Kobayashi, J. Normand, K. Raghavachari, A. Rendell, J. C. Burant, S. S. Iyengar, J. Tomasi, M. Cossi, N. Rega, J. M. Millam, M. Klene, J. E. Knox, J. B. Cross, V. Bakken, C. Adamo, J. Jaramillo, R. Gomperts, R. E. Stratmann, O. Yazyev, A. J. Austin, R. Cammi, C. Pomelli, J. W. Ochterski, R. L. Martin, K. Morokuma, V. G. Zakrzewski, G. A. Voth, P. Salvador, J. J. Dannenberg, S. Dapprich, A. D. Daniels, O. Farkas, J. B. Foresman, J. V. Ortiz, J. Cioslowski, and D. J. Fox, Gaussian, Inc., Wallingford CT, 2013.
13) Kessler M. J. "Liquid Scintillation Analysis Science and Technology", Packard Instrument Company (now Perkin Elmer), Meriden, CT, 1989.